Low core losses of nanocrystalline Fe–M–B (M=Zr, Hf, or Nb) alloys

Kiyonori Suzuki, Akihiro Makino, Akihisa Inoue, and Tsuyoshi Masumoto

Citation: Journal of Applied Physics **74**, 3316 (1993); doi: 10.1063/1.354555
View online: http://dx.doi.org/10.1063/1.354555
View Table of Contents: http://scitation.aip.org/content/aip/journal/jap/74/5?ver=pdfcov
Published by the AIP Publishing

Low core losses of nanocrystalline Fe–M–B (M=Zr, Hf, or Nb) alloys

Kiyonori Suzuki,[a] Akihiro Makino,[b] Akihisa Inoue, and Tsuyoshi Masumoto
Institute for Materials Research, Tohoku University, Sendai 980, Japan

(Received 2 November 1992; accepted for publication 18 May 1993)

Magnetic core properties, core loss, permeability, and saturation magnetic induction of bcc-nanocrystalline Fe–M–B (M=Zr, Hf, and Nb) alloys produced by annealing a melt-spun amorphous phase were investigated in a ring-shaped form with the aim of clarifying the application potential as a core material. The bcc alloys exhibit high saturation induction (B_s) from 1.49 to 1.63 T combined with high permeability (μ_e) from 22 000 to 32 000 at 1 kHz and 0.4 A/m. The bcc Fe–M–B (M=Zr, Hf, or Nb) alloys also show low core losses (W) from 1.4×10^{-1} to 2.1×10^{-1} W/kg at 50 Hz and 1.4 T and from 1.70 to 2.50 W/kg at 1 kHz and 1.0 T. The W values attained for the bcc Fe–M–B (M=Zr, Hf, and Nb) alloys are smaller by 60%–90% at 50 Hz and 1.4 T and 50%–70% at 1 kHz and 1.0 T, as compared with those for an amorphous $Fe_{78}Si_9B_{13}$ alloy in practical use as a transformer core material. The low W values for the bcc-nanocrystalline alloys are presumably due to the small anomaly factor comparable to a Co-based amorphous alloy. The comparison of the present data with those for the amorphous $Fe_{78}Si_9B_{13}$ alloy indicates that the bcc-nanocrystalline Fe–M–B (M=Zr, Hf, and Nb) alloys are promising for practical use as core materials.

I. INTRODUCTION

Recently, there has been a strong need for electromagnetic devices with a high degree of performance. Accordingly, with the aim of developing magnetic materials exhibiting high saturation induction and good soft magnetic properties, trials to improve soft magnetic properties of Fe-based amorphous alloys have been carried out for the last decade.

It is known[1] that the precipitation of fine bcc particles in Fe-based amorphous phase brings about an improvement of soft magnetic properties. It has subsequently been reported[2] that the Fe–Si–B–Nb–Cu amorphous alloys crystallize into a bcc structure with a nanoscale grain size of 10 nm and the bcc alloy exhibits good soft magnetic properties with a high saturation induction of 1.3 T. The good soft magnetic properties for the nanocrystalline alloys have been explained on the basis of the ripple theory[3] or the random anisotropy model.[4]

The present authors have recently carried out a systematic study on the development of new soft magnetic materials in Fe–M–B (M=transition metals) systems by the melt spinning technique. As a result, we have reported[5–9] that a mostly single bcc phase with nanoscale grain size forms by annealing the amorphous Fe–Zr–B, Fe–Hf–B, and Fe–M–B–Cu (M=Ti, Zr, Hf, Nb, or Ta) alloys and the bcc-nanocrystalline alloys exhibit good soft magnetic properties with a high saturation induction reaching 1.7 T. However, the soft magnetic properties reported in the previous papers were mainly obtained from the straight strip samples, with a width of about 1 mm. The use of the sample in a closed magnetic circuit form is required to evaluate the intrinsic magnetic softness and to obtain a definite conclusion on the possibility of practical use as the core materials. The aim of this paper is to examine magnetic core properties for the nanocrystalline Fe–M–B (M=Zr, Hf, or Nb) alloys in a ring-shaped form and to investigate the possibility of practical use in comparison with those for an amorphous $Fe_{78}Si_9B_{13}$ alloy, which is a core material in practical use.

II. EXPERIMENTAL PROCEDURE

Alloy ingots were prepared by arc melting in an argon atmosphere. A single-roller melt spinning method was used to produce the rapidly solidified ribbon with a cross section of about 0.02×13 mm^2. The ring-shaped sample with a size of 6 mm in inner diameter and 10 mm in outer diameter was prepared by mechanical punching. The as-quenched samples were annealed for 3.6 ks at various temperatures under no magnetic field in an evacuated state. The identification method of as-quenched and annealed structure has been described in Ref. 6. The lattice spacing was evaluated from the x-ray diffraction peak measured by the step scanning method. The diffraction angles were calibrated at each measurement, based on the diffraction angle measured for the pure Si powder (standard reference material 640a distributed by the National Bureau of Standards). In addition, a commercial $Fe_{78}Si_9B_{13}$ amorphous alloy (METGLAS™ 2605 S2) was used for comparison.

Saturation magnetostriction (λ_s) was measured for a disk-shaped sample with a diameter of 10 mm in an applied field up to 40 kA/m by using the strain gauges on both sides of the sample. Magnetic induction (B_8) and coercive force (H_c) were measured with a dc B–H loop tracer in an applied field up to 8 kA/m. Effective permeability (μ_e) and core loss (W) were measured with a vector impedance analyzer at 1 kHz under 0.4 A/m, and with an ac B–H

[a]Present address: Niigata Division, Alps Electric Co., Ltd., 1-3-5 Higashitakami Nagaoka 940, Japan.
[b]Niigata Division, Alps Electric Co., Ltd.

 0021-8979/93/74(5)/3316/7/$6.00

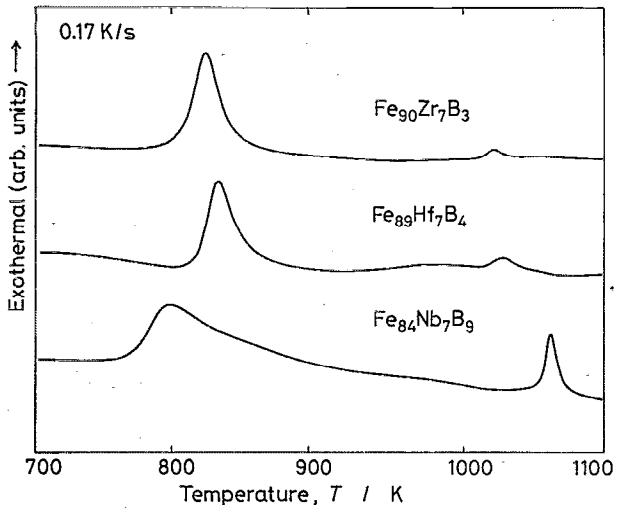

FIG. 1. DTA curves of amorphous $Fe_{90}Zr_7B_3$, $Fe_{89}Hf_7B_4$, and $Fe_{84}Nb_7B_9$ alloys.

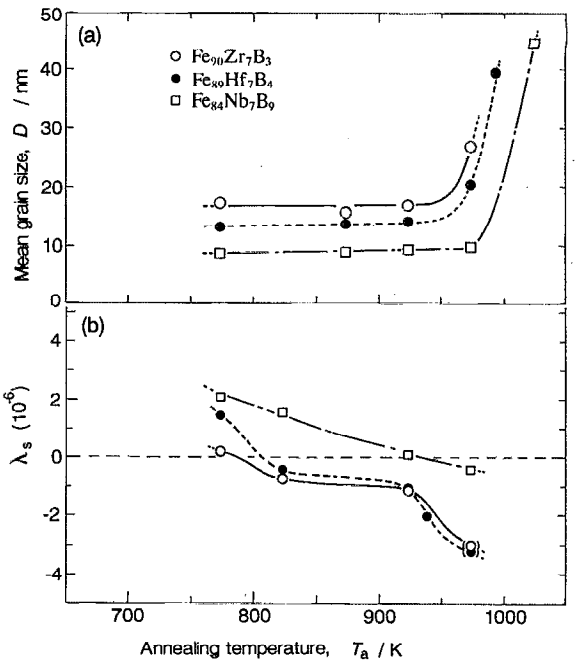

FIG. 2. Changes in mean grain size (D) and saturation magnetostriction (λ_s) as a function of annealing temperature (T_a) for 3.6 ks for amorphous $Fe_{90}Zr_7B_3$, $Fe_{89}Hf_7B_4$, and $Fe_{84}Nb_7B_9$ alloys.

analyzer under the condition of the sinusoidal magnetization. Electrical resistivity (ρ) was measured by a dc four-prove technique. Density (D_m) was measured by the Archimedian method using tetrabromoethane.

III. RESULTS AND DISCUSSIONS

A. Microstructure and magnetostriction

In the Fe–M–B ternary systems, the crystallization behavior of an amorphous $Fe_{91}Zr_7B_2$ alloy[6] has already been reported. That is, the alloy crystallizes through two stages, consisting of the first-stage change from amorphous to bcc phase and the second-stage change from bcc to α-Fe +compounds. Figure 1 shows the DTA curves of amorphous $Fe_{90}Zr_7B_3$, $Fe_{89}Hf_7B_4$, and $Fe_{84}Nb_7B_9$ alloys. Two exothermic peaks are seen on all the DTA curves, indicating that these amorphous alloys also crystallize through two stages. Furthermore, the mostly single bcc phase with a grain size smaller than 20 nm was confirmed by TEM for these samples annealed for 3.6 ks at 923 K, which is located in the temperature range between the first and second peaks on these DTA curves. The structural changes by isochronal annealing for 3.6 ks were examined by x-ray diffractometry, in order to determine an optimum annealing condition for obtaining a mostly single bcc phase for these Fe–M–B amorphous alloys. The transition of the amorphous to the bcc phase for each alloy begins identically to occur at annealing temperature (T_a) of 723 K, and is almost completed at T_a=773 K. Although no significant change in the annealed structures is seen in the T_a range from 773 to 923 K, the further increase of T_a results in a mixed structure of α-Fe and compounds (Fe_3Zr, Fe_2Hf, Fe_2Nb, and other unidentified phases). The lattice spacing of $(110)_{bcc}$ (d_{110}) for the bcc Fe–M–B alloys obtained by annealing was measured to be 0.2030 nm for $Fe_{90}Zr_7B_3$ and $Fe_{89}Hf_7B_4$ and 0.2032 nm for $Fe_{84}Nb_7B_9$ at T_a=773 K. These d_{110} values are larger than that (0.2027 nm) for pure α-Fe, and decrease gradually to 0.2028 nm with increasing T_a to 1173 K. The tendency for d_{110} indicates that the dissolution amount of the solute elements in the bcc phase decreases with increasing T_a through the decomposition of the nonequilibrium bcc phase, which is saturated with the solute elements.

Figures 2(a) and 2(b) shows the mean grain size (D) and saturation magnetostriction (λ_s) as a function of T_a for amorphous Fe–M–B (M=Zr, Hf, or Nb) alloys. D was estimated by using Scherrer's equation[10] from the half-width of $(110)_{bcc}$ diffraction peak obtained by the step scanning method. Broadening of diffraction lines due to a width of x-ray source was removed by Warren's method,[10] on the basis of the half-width value measured for a single crystal Si. In Fig. 2(b), the plot marked in parentheses indicates that the magnetostriction is unsaturated under an applied field of 40 kA/m. D values for the bcc $Fe_{90}Zr_7B_3$, $Fe_{89}Hf_7B_4$ and $Fe_{84}Nb_7B_9$ alloys obtained by annealing at T_a=773 K are as small as 18, 14, and 9 nm, respectively. When T_a is below 950 K, all the D values are independent of T_a. However, the D values are strongly dependent on T_a in the temperature range higher than 950 K. Considering that the phase transition from bcc to α-Fe +compounds is confirmed at T_a=973 K, the grain growth of the bcc phase appears to take place accompanied by the decomposition of the bcc phase. λ_s shows positive values ranging from 0.2×10^{-6} to 2.2×10^{-6} at T_a=773 K and changes to negative values of 0.5×10^{-6} to 3.6×10^{-6} passing through zero with further increasing T_a. The change in λ_s with T_a is presumed to reflect the process in which λ_s approaches the value of polycrystalline α-Fe(-4.4×10^{-6}). This presumption is also supported from the re-

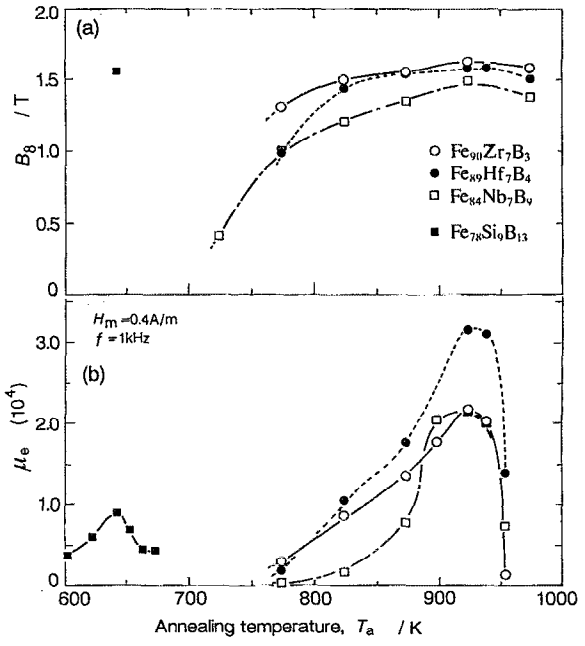

FIG. 3. Changes in B_s and μ_e at 1 kHz and 0.4 A/m as a function of T_a for 3.6 ks for amorphous $Fe_{90}Zr_7B_3$, $Fe_{89}Hf_7B_4$, and $Fe_{84}Nb_7B_9$ alloys.

sult that the decrease of solute contents in the bcc phase is recognized through the decrease of d_{110}.

B. Soft magnetic properties

Figures 3(a) and 3(b) show the changes in B_8 and μ_e at 1 kHz and 0.4 A/m as a function of T_a for a constant annealing time of 3.6 ks for the amorphous $Fe_{90}Zr_7B_3$, $Fe_{89}Hf_7B_4$ and $Fe_{84}Nb_7B_9$ alloys. The data of the amorphous $Fe_{78}Si_{13}B_9$ alloy are also shown for comparison. Both B_8 and μ_e of the Fe–M–B (M=Zr, Nb, or Hf) alloys increase in the T_a range from 723 to 773 K, where the structural change from the amorphous to the bcc phase is observed. μ_e of the Fe–M–B (M=Zr, Nb, or Hf) alloys reaches maximum values of 22 000–32 000 at T_a=923 K and then decreases rapidly at T_a=950 K, where the bcc phase decomposes to α-Fe+compounds. The decrease in μ_e associated with the decomposition of the bcc phase is explained by the formation of the compounds that have larger magnetocrystalline anisotropy, as well as by the coarsening of the bcc grain, leading to the increase in the reduced apparent anisotropy resulting from the grain size refinement.

As shown in Figs. 2 and 3, the T_a at which the highest μ_e is obtained does not agree with T_a, leading to zero magnetostriction for the nanocrystalline $Fe_{90}Zr_7B_3$ and $Fe_{89}Hf_7B_4$ alloys. Considering that excellent soft magnetic properties are obtained in the case where both λ_s and magnetocrystalline anisotropy have small values, the present result suggests that an effective anisotropy for the nanocrystalline Fe–M–B alloys decreases with approaching T_a to 923 K, where the highest μ_e is obtained. Herzer has evaluated[4] the average anisotropy ($\langle K\rangle$) for nanocrystalline soft magnetic alloys on the basis of the random anisotropy model and reported that the $\langle K\rangle$ value for three-dimensional samples is expressed by Eq. (1),

$$\langle K\rangle \simeq K_1^4 D^6/A^3. \tag{1}$$

Here, K_1 is the magnetocrystalline anisotropy constant of the grains, D is the grain size, and A is the exchange stiffness. The equation has been derived from the assumption that the randomly oriented grains are perfectly coupled through the exchange interaction. It has been pointed out[11,12] that the decrease in the apparent anisotropy resulting from the refinement of grain size does not occur effectively, when a nonmagnetic phase exists along the grain boundary and the exchange coupling between individual grains is inhibited. When the $\langle K\rangle$ value for the nanocrystalline Fe–M–B alloys is assumed to be expressed by Eq. (1), the $\langle K\rangle$ value is mainly dominated by D, however, the D value for the nanocrystalline Fe–M–B alloys remains almost constant in the T_a range of 773–923 K. This indicates that the $\langle K\rangle$ value for the nanocrystalline Fe–M–B alloys is dependent on K_1 and A. It is very difficult to evaluate K_1 for the bcc grain, and hence the change in K_1 with T_a remains unknown. On the other hand, the effective A value is presumed as follows; Since the crystallization temperature of the amorphous Fe–M–B alloys is about 800 K, it is reasonable to consider that a relatively large amount of amorphous phase exists along the grain boundary in the nanocrystalline bcc alloys obtained at low T_a. The increase in B_8 with approaching T_a to 923 K for the nanocrystalline alloys shown in Fig. 3(a) is presumably because the volume fraction of the residual amorphous phase with low magnetization decreases through the crystallization into the bcc phase. The Fe concentrations of the Fe–M–B amorphous alloys are as high as 84%–90%, and T_c lies around room temperature because of the Invar effect. Accordingly, it is thought that the residual existence of the amorphous phase along the grain boundaries of the bcc phase causes the decrease of effective A between the bcc grains, leading to the increase in $\langle K\rangle$.

More recently, the present authors have examined[13] the temperature dependence of μ_e for the nanocrystalline $Fe_{89}Hf_7B_4$ alloy, and confirmed that the μ_e value of the nanocrystalline bcc phase obtained at T_a below 873 K increase when the measurement temperature decrease from room temperature to 77 K. This change is induced, presumably because the increase in the magnetization for the residual amorphous phase with decreasing measurement temperature causes the increase in effective A, leading to the decrease in $\langle K\rangle$. It is therefore said that the residual amorphous phase along the grain boundaries of the bcc phase inhibits the effective generation of exchange coupling between the bcc grains for the nanocrystalline $Fe_{89}Hf_7B_4$ alloy obtained by annealing at T_a below 873 K. Thus, the soft magnetic properties of the nanocrystalline Fe–M–B alloys are also dominated by the existence of the grain boundary phase that affects the effective A value, in addition to D and λ_s.

It is to be noticed that the highest μ_e of the nanocrystalline Fe–M–B alloys is about three times as high as that (9000) for the amorphous $Fe_{78}Si_9B_{13}$ alloy annealed for 3.6

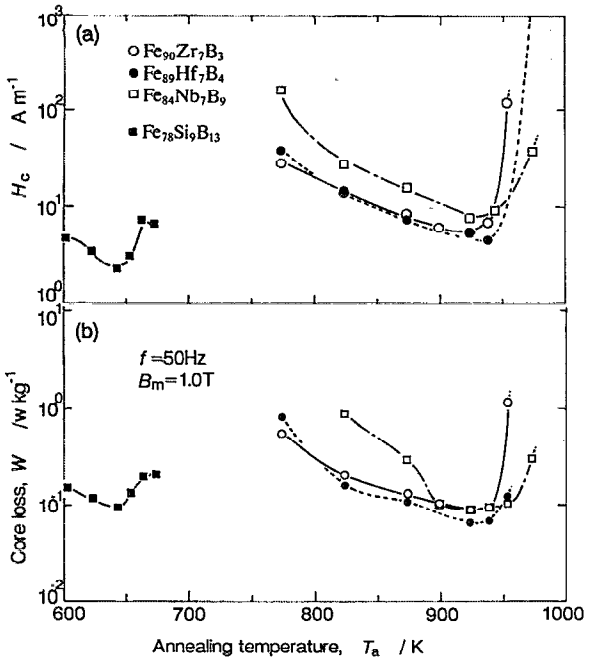

FIG. 4. Changes in coercive force (H_c) and core loss (W) at 50 Hz and 1.0 T as a function of T_a for 3.6 ks for amorphous $Fe_{90}Zr_7B_3$, $Fe_{89}Hf_7B_4$ and $Fe_{84}Nb_7B_9$ alloys.

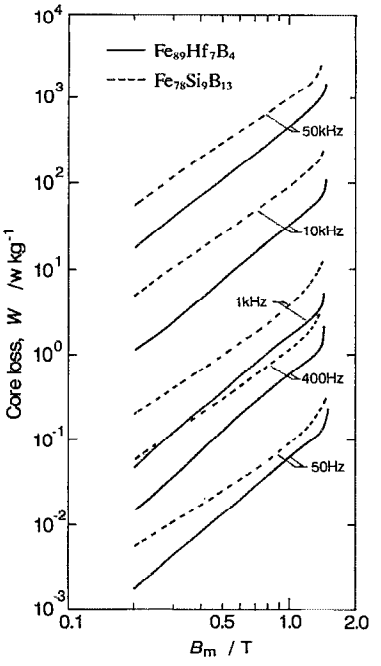

FIG. 5. Relation between W and maximum induction field (B_m) for a bcc $Fe_{89}Hf_7B_4$ alloy produced by annealing the melt-spun amorphous phase at 923 K for 3.6 ks. The data of the amorphous $Fe_{78}Si_9B_{13}$ alloy are also shown for comparison.

ks at an optimum T_a of 643 K, being equivalent to that ($\simeq$25 000)[14] for the amorphous Co–Fe–Si–B alloys, with the same sample geometry as that used in the present work. The B_8 value for the nanocrystalline Fe–M–B alloys at T_a=923 K, where the maximum μ_e value obtained is 1.63 T for M=Zr, 1.59 T for M=Hf, and 1.49 T for M=Nb, being comparable to that (1.56 T) for the amorphous Fe–Si–B alloy. The B_8 value for these optimum annealed samples was confirmed to agree with the $4\pi I_s$ value measured with a vibrating-sample magnetometer. As shown in Fig. 2(b), the magnitude of λ_s of the nanocrystalline Fe–M–B alloys is less than 1.2×10^{-6} at Ta=923 K, where the maximum μ_e is obtained. The λ_s value is smaller than 5% of that (27×10^{-6})[15] for the amorphous $Fe_{78}Si_9B_{13}$ alloy, being equivalent to that ($<1\times10^{-6}$)[14] for the amorphous Co–Fe–Si–B alloys and seems to be a major reason for the higher μ_e values for the nanocrystalline Fe–M–B (M=Zr, Hf, and Nb) alloys, in comparison with the amorphous Fe–Si–B alloy.

Figures 4(a) and 4(b) show the coercive force (H_c) and the core loss (W) at 50 Hz and 1.0 T, respectively, as a function of T_a, for the nanocrystalline Fe–M–B (M=Zr, Hf, and Nb) alloys, along with the data for the commercial amorphous Fe–Si–B alloy. For all the alloys, H_c and W have a similar tendency against T_a and show minima at around T_a=923 K for the nanocrystalline Fe–M–B alloys, and at T_a=643 K for the amorphous Fe–Si–B alloy. The optimum T_a leading to the minimum values of H_c and W agrees with that at which the maximum μ_e is obtained in Fig. 3(b). Although the H_c for the amorphous Fe–Si–B alloy annealed at T_a=643 K is smaller than that for the nanocrystalline Fe–M–B alloys annealed at optimum T_a, the minimum W value is 8.9×10^{-2} W/kg for M=Zr, 6.6×10^{-2} W/kg for M=Hf, and 9.0×10^{-2} W/kg for M=Nb, being lower than that (9.7×10^{-2} W/kg) for the amorphous Fe–Si–B alloy.

The frequency (f) and B_m dependence of core loss was examined for the nanocrystalline $Fe_{89}Hf_7B_4$ alloy prepared by annealing the amorphous phase at 923 K for 3.6 ks, in comparison with the data for the amorphous $Fe_{78}Si_9B_{13}$ alloy subjected to the optimum heat treatment. W values in the frequency range of 50 Hz–50 kHz are plotted as a function of B_m in Fig. 5. W of the nanocrystalline Fe–Hf–B alloy is smaller than that for the amorphous Fe–Si–B alloy at each frequency in the entire B_m range. The W values for the nanocrystalline Fe–Hf–B and amorphous Fe–Si–B alloys at 1.0 T were replotted as a function of f in Fig. 6, in order to compare the frequency dependence of core loss. The data for the nanocrystalline $Fe_{90}Zr_7B_3$ and $Fe_{84}Nb_7B_9$ alloys subjected to the optimum annealing treatment are shown in Fig. 6, where the catalog data[15] for the amorphous $Fe_{78}Si_9B_{13}$ (METGLAS™ 2605 S2) and $Fe_{77}Si_5B_{16}Cr_2$ (METGLAS™ 2605 S3A) alloys are also shown for comparison. When the present result for the amorphous Fe–Si–B alloy is compared with the catalog data, the sample annealed under no applied field shows lower W values in the frequency range above 400 Hz. On the other hand, the catalog data for the sample annealed under the longitudinal applied field are lower at f=60 Hz. This difference in W is due to the change in the gradient in the log W vs log f curve. The larger gradient in the log W vs log f curve for the catalog data seems to result from the decrease in static hysteresis loss governing the W values in a low-frequency range and the increase in anomalous eddy

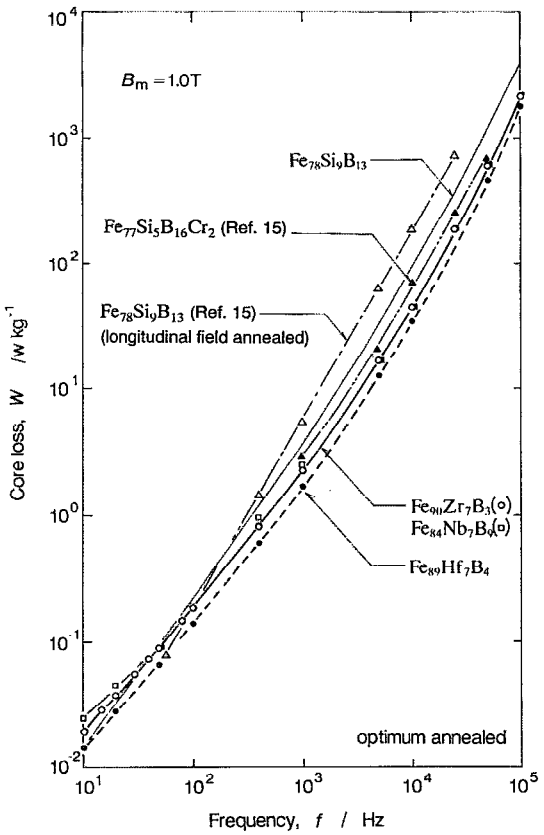

FIG. 6. Relation between W at $B_m = 1.0$ T and frequency (f) for nanocrystalline $Fe_{90}Zr_7B_9$, $Fe_{89}Hf_7B_4$, and $Fe_{84}Nb_7B_9$ alloys produced by annealing the melt-spun amorphous phase for 3.6 ks at 923 K. Present data for the amorphous $Fe_{78}Si_9B_{13}$ alloy and catalog data (see Ref. 15) for the amorphous $Fe_{78}Si_9B_{13}$ and $Fe_{77}Si_5B_{16}Cr_2$ alloys are also shown for comparison.

current loss in a high-frequency range. This change is presumably attributed to the growth of domains with 180° wall induced by the longitudinal field annealing. Although the W values for the nanocrystalline $Fe_{90}Zr_7B_3$ and $Fe_{84}Nb_7B_9$ alloys are larger than that for the amorphous $Fe_{78}Si_9B_{13}$ alloy in the f range below 50 Hz, all the nanocrystalline Fe–M–B (M=Zr, Hf, or Nb) alloys have lower W values in the wide f range from 50 Hz to 100 kHz, in comparison with the amorphous Fe–Si–B alloy, subjected to annealing under no applied field. Furthermore, the W values for the nanocrystalline Fe–M–B alloys are obviously smaller than the catalog data for the amorphous Fe–Si–B–Cr alloy designed for the high-frequency use of >1 kHz.

Typical magnetic properties for the bcc Fe–M–B (M=Zr, Hf, or Nb) alloys annealed for 3.6 ks at 923 K under no applied field are summarized in Table I, where the data for the amorphous Fe–Si–B alloy are also shown for comparison. The low core losses combined with high values of B_s and μ_e and small magnetostriction lead to an expectation that the present nanocrystalline Fe–M–B alloys may be used as a core material in high-frequency transformers, in which Fe–Si–B based amorphous alloys are presently being used.[16]

C. Loss separation

The basic loss separation was tried at a constant B_m of 1.0 T, to gain a better understanding of the difference in core losses between the nanocrystalline Fe–M–B alloys and the amorphous Fe–Si–B alloy. The static hysteresis loss (W_h) is evaluated to be 1.75 mJ/kg for the nanocrystalline $Fe_{90}Zr_7B_3$ alloy, and 1.16 mJ/kg for the amorphous $Fe_{78}Si_9B_{13}$ alloy from the area of dc B–H loop at B_m=1.0 T. The classical eddy current loss (W_c) is calculated by Eq. (2),

$$W_c = (\pi t f B_m)^2/6\rho D_m. \quad (2)$$

Here, t is the thickness of the sheet, f is the frequency, B_m is the maximum flux density, ρ is the electrical resistivity, and D_m is the density. The separated core loss in core losses per cycle for the nanocrystalline $Fe_{90}Zr_7B_3$ and amorphous $Fe_{78}Si_9B_{13}$ alloys is shown in Figs. 7 and 8, respectively. Although the W_c for the amorphous Fe–Si–B alloy with a higher ρ value of 137×10^{-8} Ω m is smaller than that for the bcc Fe–Zr–B alloy, with ρ of 44×10^{-8}

TABLE I. Magnetic properties (W, B_s, μ_e, H_c, and λ_s), electrical resistivity (ρ), sample thickness (t), and density (D_m) for nanocrystalline $Fe_{90}Zr_7B_3$, $Fe_{89}Hf_7B_4$, and $Fe_{84}Nb_7B_9$ and amorphous $Fe_{78}Si_9B_{13}$ alloys.

Structure	$Fe_{90}Zr_7B_3$ Nanocrystalline	$Fe_{89}Hf_7B_4$ Nanocrystalline	$Fe_{84}Nb_7B_9$ Nanocrystalline	$Fe_{78}Si_9B_{13}$ Amorphous
$W_{14/50}$ [a] (W/kg)	0.21	0.14	0.19	0.24
$W_{10/400}$ [a] (W/kg)	0.82	0.61	0.97	1.22
$W_{10/1k}$ [a] (W/kg)	2.27	1.70	2.50	3.72
$W_{2/100k}$ [a] (W/kg)	79.7	59.0	75.7	168
B_s (T)	1.63	1.59	1.49	1.56
μ_e [b]	22 000	32 000	22 000	9000
H_c (A/m)	5.6	5.6	8.0	2.4
$\lambda_s\times10^6$	−1.1	−1.2	0.1	27[c]
$\rho\times10^8$ (Ω m)	44	48	58	137[c]
t (μm)	18	17	22	20
$D_m\times10^{-3}$ (kg/m^3)	7.62	8.46	7.74	7.18[c]

[a] $W_{\alpha/\beta}$ is the core loss at $\alpha\times10^{-1}$ T and β Hz.
[b] f=1 kHz, H_m=0.4 A/m.
[c] Reference 15.

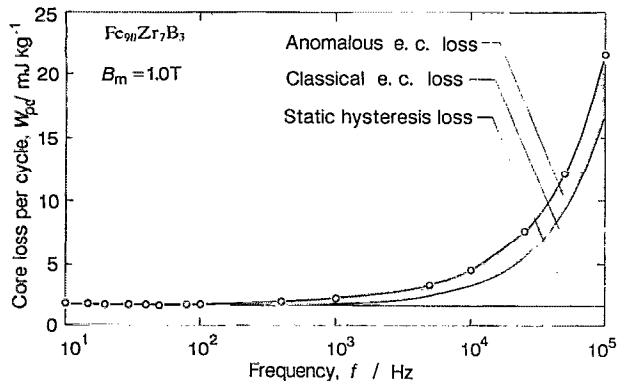

FIG. 7. Relation between separated core loss in core losses per cycle (W_{pc}) and f for a nanocrystalline $Fe_{90}Zr_7B_3$ alloy.

Ω m in the entire f range, the anomalous eddy current loss ($W_a = W - W_h \cdot f - W_c$) of the amorphous Fe–Si–B alloy is much higher than that of the nanocrystalline Fe–Zr–B alloy, leading to the lower values of the total eddy current loss ($W_{et} = W_c + W_a$) for the nanocrystalline Fe–Zr–B alloy. The anomaly factor ($\eta = W_{et}/W_c$) at 50 kHz and 1.0 T is evaluated to be 1.4 for the nanocrystalline alloy, with a dc remanence ratio of 0.44 and 5.7 for the amorphous alloy with a dc remanence ratio of 0.37. The small η value near 1 for the nanocrystalline alloy is comparable to that (1.5)[17] at 50 kHz and 0.4 T for the commercial amorphous $Co_{65}Fe_4Ni_2Si_{15}B_{14}$ alloy (METGLAS™ 2714 A) annealed under no applied field. The small anomaly factor comparable to that for the Co-based amorphous alloy seems to be a major reason for the low core losses for the nanocrystalline Fe–M–B (M=Zr, Hf, and Nb) alloys.

It is known that the η value is closely related to the magnetic domain structure of alloys, particularly the spacing of domains with 180° wall. It is therefore said that the observation of domain structure is essential for clarification of the reason for the difference in η between the nanocrystalline Fe–M–B alloys and the amorphous Fe–Si–B alloy. There is no report on the domain structure of the nanocrystalline Fe–M–B alloys, however, the curved domains with a width of about 100 μm separated by 180° walls have been observed[18] for a nanocrystalline $Fe_{73.5}Si_{13.5}B_9Nb_3Cu_1$ alloy with low core losses comparable to those for Co-based amorphous alloys with zero magnetostriction. The feature is similar to that for conventional amorphous soft magnetic alloys. The similarity in the domain structure between the nanocrystalline and amorphous soft magnetic alloys suggests that the reason for the difference in η between the nanocrystalline Fe–M–B alloys and the amorphous Fe–Si–B alloy is due to the factors that affect domain structure, e.g., magnetostriction or local anisotropy, rather than the intrinsic difference in structure between the noncrystalline and the amorphous phases.

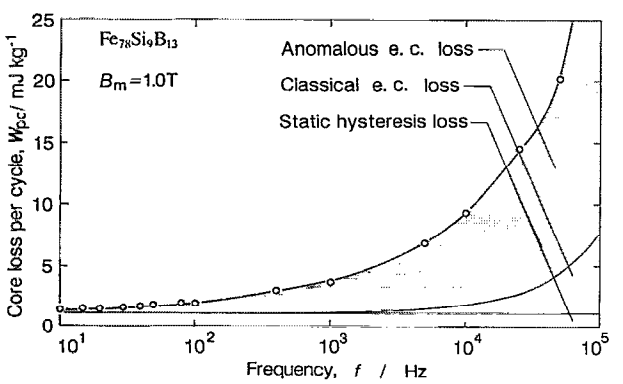

FIG. 8. Relation between separated core loss in core losses per cycle (W_{pc}) and f for an amorphous $Fe_{78}Si_9B_{13}$ alloy.

Inomata *et al.* have reported[19] that the anomaly factor in a frequency range of 10–50 kHz for the amorphous Fe–Si–B–Nb alloys is proportional to λ_s, and the η value decreases from 7.5 to 1.6 with decreasing λ_s from 30×10^{-6} to 7×10^{-6}. Considering that the η and λ_s values are 1.4 and 1.1×10^{-6}, respectively, for the nanocrystalline Fe–Zr–B alloy and 5.7 and 27×10^{-6}, respectively, for the amorphous Fe–Si–B alloy, the difference in η observed in the present study can be explained by taking the difference in λ_s into consideration. Thus, it is said that the study on the influence of magnetostriction on domain structure is required for the clarification of the reason for the low core losses in the high-frequency range for the nanocrystalline Fe–M–B alloys.

IV. CONCLUSION

The magnetic core properties of the bcc Fe–M–B (M =Zr, Hf, or Nb) alloys with nanoscale grain sizes of 10–20 nm were examined for the ring-shaped samples. The results obtained are summarized as follows.

(1) The nanocrystalline Fe–M–B (M=Zr, Hf, or Nb) alloys produced by annealing the melt-spun amorphous phase for 3.6 ks at 923 K exhibit high B_s and μ_e values of 1.49–1.63 T and 22 000–32 000 at 1 kHz, respectively. The μ_e values are about three times as high as that (9000) for the amorphous $Fe_{78}Si_9B_{13}$ alloy, being comparable to Co-based amorphous alloys.

(2) In the frequency range from 50 Hz to 100 kHz, the nanocrystalline Fe–M–B (M=Zr, Hf, or Nb) alloys exhibit core losses lower than that for the amorphous $Fe_{78}Si_9B_{13}$ alloy. The values are smaller by 60%–90% at 50 Hz and 50%–70% at 1 kHz, as compared with those for the amorphous Fe–Si–B alloy. The low core losses combined with high B_s and high μ_e values allow us to expect that the bcc-nanocrystalline Fe–M–B (M=Zr, Hf, or Nb) alloys could be useful for various types of transformers in which amorphous Fe–Si–B alloys are presently being used.

(3) The small anomaly factor equivalent to a Co-based amorphous alloy was confirmed for the nanocrystalline $Fe_{90}Zr_7B_3$ alloy at 50 kHz, and is thought to be the main reason for the low core losses for the nanocrystalline Fe–M–B (M=Zr, Hf, or Nb) alloys.

ACKNOWLEDGMENTS

The authors would like to thank Toshifumi Hasegawa of Iwatsu Electric Co., Ltd. for generous permission to use

an ac B–H analyzer. We also acknowledge Masayuki Kido of Iwatsu Electric Co., Ltd. for the technical suggestions in core loss measurements.

[1] R. Hasegawa, G. E. Fish, and V. R. V. Rammanan, *Proceedings of the 4th International Conference on Rapidly Quenched Metals*, edited by T. Masumoto and K. Suzuki (Japan Institute of Metals, Sendai, 1981), p. 929.
[2] Y. Yoshizawa, S. Oguma, and K. Yamauchi, J. Appl. Phys. **64**, 6044 (1988).
[3] H. Hoffman, J. Appl. Phys. **35**, 1790 (1964).
[4] G. Herzer, Mat. Sci. Eng. A **113**, 1 (1991).
[5] K. Suzuki, N. Kataoka, A. Inoue, A. Makino, and T. Masumoto, Mat. Trans. JIM **31**, 743 (1990).
[6] K. Suzuki, A. Makino, N. Kataoka, A. Inoue, and T. Masumoto, Mat. Trans. JIM **32**, 93 (1991).
[7] A. Makino, K. Suzuki, A. Inoue, and T. Masumoto, Mat. Trans. JIM **32**, 551 (1991).
[8] K. Suzuki, A. Makino, A. Inoue, and T. Masumoto, Jpn. J. Appl. Phys. **30**, L1729 (1991).
[9] K. Suzuki, A. Makino, A. Inoue, and T. Masumoto, J. Appl. Phys. **70**, 6232 (1991).
[10] B. D. Cullity, *Elements of X-ray Diffraction*, 2nd ed. (Addison-Wesley, Reading, MA, 1959), p. 262.
[11] G. Herzer, IEEE Trans. Magn. **25**, 3327 (1989).
[12] K. Suzuki, M. Kikuchi, A. Makino, A. Inoue, and T. Masumoto, Mat. Trans. JIM **32**, 961 (1991).
[13] K. Suzuki, A. Makino, A. Inoue, and T. Masumoto, J. Jpn. Inst. Metals (in press).
[14] K. Hayashi, M. Hayakawa, Y. Ochiai, H. Matsuda, W. Ishikawa, and K. Aso, J. Appl. Phys. **55**, 3028 (1984).
[15] METGLAS™, Magnetic Alloys Technically Superior (Allied Signal Inc., Parsippany, NJ), p. 14.
[16] METGLAS™ JISEI ZAIRYO (Nippon Amorphous Metals Co., Ltd., Tokyo, 1985), p. 25 (in Japanese).
[17] C. S. Tsai, W. J. Yang, M. S. Leu, and C. S. Lin, J. Appl. Phys. **70**, 5846 (1991).
[18] R. Schäfer, A. Hubert, and G. Herzer, J. Appl. Phys. **69**, 5325 (1991).
[19] K. Inomata, M. Hasegawa, T. Kobayashi, and T. Sawa, J. Appl. Phys. **54**, 6553 (1983).